Supplementary Information.

Superhydrophobic μ-Pillars via Simple and Scalable SLA 3D-Printing: The Stair-Case Effect and their Wetting Models.

José Bonilla-Cruz, Jo Ann C. Sy, Tania E. Lara-Ceniceros, Julio C. Gaxiola-López, Vincent García, Blessie Basilia, and Rigoberto C. Advincula*

S1. Theoretical Models

S1.1 Wenzel wetting state

This model describes the homogeneous wettability regime of a rough surface, which happens when the liquid penetrates into the asperities and interstices of the surface, making contact with the base of the protrusions. This wetting regime is described by the equation:[1]

$$\cos(\theta) = r \cos\theta_0$$

Where θ is the apparent CA of the surface which corresponds to a stable equilibrium state, which means a minimum energy state for the rough surface system. While θ_0, is the contact angle for the smooth surface and is calculated using the Young equation.[2] The roughness ratio, r, is a measure of how roughness affects the wetting behavior of the surface. The roughness ratio is calculated as the ratio of real solid/liquid contact area to the apparent or projected solid/liquid interface. So, for a rough surface, $r > 1$.

This model indicates that the roughness of a surface intensifies its intrinsic wetting behavior which depends on its chemical nature and intermolecular forces. In other words, a hydrophobic smooth surface ($\theta_0 > 90°$) will be more hydrophobic (will have greater CA) as the roughness ratio increases. On the other hand, a hydrophilic surface ($\theta_0 < 90°$) will be more hydrophilic (lower CA) as the roughness ratio magnifies. Nevertheless, it is important to mention that SHS under Wenzel wetting state have not been reported, indicating a limitation of the Wenzel model.

S1.2 Cassie-Baxter Wetting state

In the case of a heterogeneous wetting state, due to air-pockets trapped in the asperities of a rough surface, the Wenzel equation becomes insufficient, on account of the necessity of a model that measure the apparent CA when several materials are involved. When a liquid propagates over a surface the original interface is destroyed. This process implies the increment or decrement of the total free energy of the system in order to overcome the surface free energy. The liquid propagation will extend until reach a state of minimum energy.[3,4] A heterogeneous interface can be obtained if a state of minimum energy is reached before the penetration of the liquid into the asperities of rough surfaces. This wetting state can be described by the Cassie-Baxter model:[5]

$$\cos(\theta) = \phi \cos(\theta_0) + \phi - 1$$

Where ϕ is the fraction of projected solid area in contact with the liquid, whose calculation for the case of square pillars in a regular array can be observed in **Figure S1.** The Cassie-Baxter model represents an approximation of the real CA and can present great deviations and imprecisions, so its utilization is reliable for some specific geometries.[6–8] In the hypothetical case that $\phi = 0$, the θ value becomes 180°, which theoretically means that the reduction of the solid/liquid contact area promotes the superhydrophobic properties. When a heterogeneous wetting state (Cassie-Baxter state) is destroyed and turns into a homogeneous wetting state (Wenzel state), is improbable that the system recovers its heterogeneous interface due to the great amount of activation energy needed for the transition.[9]

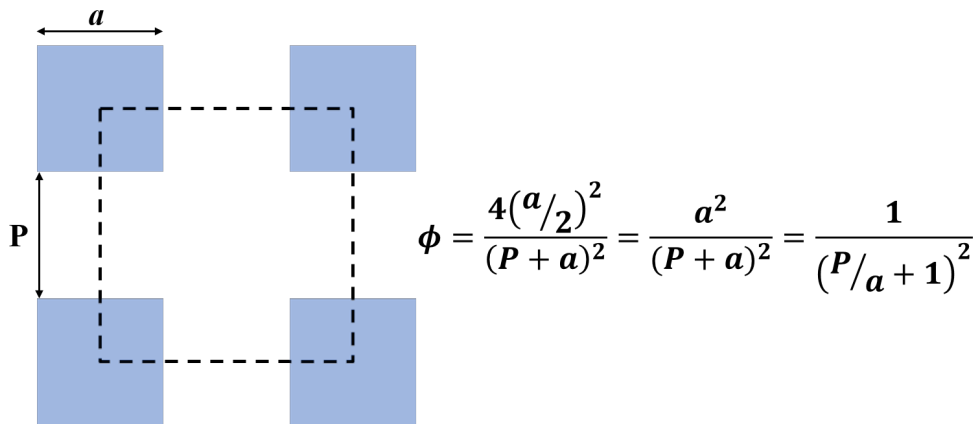

Fig. S1. Definition of the fraction of solid/liquid contact area, ϕ.

S1.3 Nagayama et al. model for intermediate wetting state

The wetting state of a system is commonly described by the static CA o CAH, putting aside the real wetting regime of the surface, which can be different from the Wenzel and Cassie-Baxter states.

Nagayama *et al.*[10] developed a wetting model that includes the description of the intermediate wetting state between homogeneous (Wenzel) and heterogeneous (Cassie-Baxter) wetting regime for a rough surface. This model is based on a thermodynamic method of minimization of energy. This intermediate wetting state has been reported and has been observed on the surface of lotus.[11] The CA based on the intermediate wetting model depends of the geometrical parameters and a new factor, f, called effective wetting ratio. This ratio can have values between 0 and 1. Further, agrees with the classical Wenzel and Cassie-Baxter models for $f = 1$ and $f = 0$, respectively. Furthermore, determines the proportion of liquid that wets into the rough surface.

The equation proposed in this model to describe the wetting phenomena arise from a method of minimization of surface free energy and the classical Young, Wenzel and Cassie-Baxter equations. The Nagayama *et al.* model is shown below:

$$\cos\theta = \phi_{sl}\cos\theta_0 + \phi_{lv}\cos 180°$$

Where ϕ_{sl} and ϕ_{lv} are the ratio of real solid/ liquid and liquid/vapor contact area with respect to the projected area, respectively. The ratios are the defined as:

$$\phi_{sl} = \phi + (r - \phi)f$$
$$\phi_{lv} = (1 - \phi)(1 - f)$$

Where r is the roughness ratio that comes from the Wenzel model, and is calculated as the area ratio of real solid/liquid interface to flat surface, as mentioned before (**see Section S1.1**).

For $f = 1$, ϕ_{sl} becomes equal to r, while ϕ_{lv} becomes 0, which is in good agreement with Wenzel state due to the absence of trapped air-pockets between the liquid and the surface. On the other hand, for $f = 0$, ϕ_{sl} becomes equal to ϕ, while ϕ_{lv} becomes $1 - \phi$, which agrees with the Cassie-Baxter model. In contrast, when $0 < f < 1$, an intermediate wetting state is observed, while $\phi < \phi_{sl} < r_w$, and $0 < \phi_{lv} < 1 - \phi$.

The effective wetting ratio, f, is calculated empirically as shown:

$$f = 1 - \phi^{D-2}$$

Where D, is the fractal dimension of the system obtained from gray scale images using a box counting method. In Nagayama *et al.* work, the fractal dimension took a value of 2.4 for a porous silicon structure. In contrast, the fractal dimension calculated for a patterned microstructured silicon surface was 2.2.

It is noteworthy the great range of potential application of the model, that includes the Wenzel and Cassie-Baxter states, as well as the intermediate state

Table S1. Static, advancing, receding, and hysteresis contact Angles (in deg.) corresponding to silanized micro-PLS, 3D printed at two orientations (tilted and horizontal), and at three resolutions (low, medium, and high).

Tag	θ_S	θ_A	θ_R	θ_H	Tag	θ_S	θ_A	θ_R	θ_H
TH_flat	112 ± 1 [a]	125 ± 1 [a]	63 ± 1 [a]	63 ± 1 [a]	FH_flat	108 ± 1 [a]	126 ± 1 [a]	49 ± 1 [a]	77 ± 1 [a]
TH_cylinder	146 ± 1	73 ± 1	45 ± 1 [a]	28 ± 1 [a]	FH_cylinder	128 ± 1 [a]	136 ± 3 [a]	88 ± 1 [a]	47 ± 1
TH_cone	**157 ± 1**	**170 ± 2**	**153 ± 1**	**17 ± 1**	FH_cone	146 ± 2	154 ± 1	118 ± 1 [a]	35 ± 1
TH_tulip	**150 ± 1**	**157 ± 2**	**142 ± 1**	**15 ± 1**	**FH_tulip**	**154 ± 1**	**155 ± 1**	**136 ± 1**	**19 ± 1**
TH_mushroom	**150 ± 1**	**163 ± 1**	**140 ± 1**	**23 ± 1**	**FH_mushroom**	**152 ± 1**	**156 ± 1**	**144 ± 2**	**12 ± 1**
TH_M. mouse	152 ± 1	166 ± 1	107 ± 1 [a]	59 ± 1	FH_M. mouse	147 ± 1	165 ± 3	124 ± 1 [a]	41 ± 2
TH_cubic	157 ± 2	159 ± 2	121 ± 3 [a]	38 ± 2	FH_cubic	144 ± 4	147 ± 1	127 ± 1 [a]	19 ± 1
TH_pyramid	155 ± 1	165 ± 2	134 ± 4 [a]	31 ± 3	**FH_pyramid**	**160 ± 4**	**163 ± 2**	**149 ± 5**	**14 ± 3**
TH_spiral	**152 ± 1**	**159 ± 1**	**151 ± 4**	**8 ± 3**	FH_spiral	154 ± 1	165 ± 3	126 ± 2 [a]	19 ± 2
TH_sphere	**154 ± 1**	**172 ± 1**	**143 ± 1**	**29 ± 1**	FH_sphere	148 ± 1	151 ± 1	130 ± 1	21 ± 1
TH_pine	139 ± 1 [a]	162 ± 2 [a]	113 ± 2 [a]	49 ± 2 [a]	FH_pine	150 ± 1	140 ± 3 [a]	70 ± 2 [a]	70 ± 2
TM_flat	113 ± 1 [a]	115 ± 1 [a]	64 ± 4 [a]	50 ± 3 [a]	FM_flat	122 ± 4 [a]	127 ± 2 [a]	60 ± 2 [a]	67 ± 2 [a]
TM_cylinder	137 ± 1 [a]	110 ± 3 [a]	64 ± 4 [a]	46 ± 3 [a]	FM_cylinder	120 ± 1 [a]	111 ± 2 [a]	63 ± 6 [a]	47 ± 4
TM_cone	155 ± 1	156 ± 2	128 ± 6 [a]	28 ± 4	FM_cone	158 ± 2	157 ± 3	66 ± 1 [a]	91 ± 2
TM_tulip	**151 ± 1**	**168 ± 2**	**145 ± 3**	**23 ± 3**	FM_tulip	144 ± 1	152 ± 3	120 ± 1 [a]	31 ± 2
TM_mushroom	**152 ± 3**	**164 ± 2**	**142 ± 4**	**22 ± 3**	FM_mushroom	148 ± 1	159 ± 2	132 ± 1	27 ± 2
TM_M. mouse	**164 ± 1**	**170 ± 2**	**146 ± 1**	**24 ± 2**	FM_M. mouse	147 ± 1	166 ± 5	137 ± 1	16 ± 3
TM_cubic	**160 ± 3**	**167 ± 2**	**157 ± 3**	**10 ± 2**	FM_cubic	145 ± 3	156 ± 4	115 ± 1 [a]	40 ± 3
TM_pyramid	**157 ± 3**	**168 ± 2**	**156 ± 4**	**12 ± 3**	**FM_pyramid**	**153 ± 2**	**165 ± 2**	**146 ± 2**	**19 ± 2**
TM_spiral	**154 ± 1**	**164 ± 1**	**149 ± 6**	**15 ± 4**	FM_spiral	144 ± 1	166 ± 2	114 ± 2 [a]	53 ± 2
TM_sphere	**151 ± 1**	**167 ± 2**	**147 ± 1**	**20 ± 1**	FM_sphere	145 ± 1	164 ± 2	134 ± 1 [a]	29 ± 2
TM_pine	147 ± 1	111 ± 1 [a]	64 ± 4 [a]	47 ± 3 [a]	FM_pine	128 ± 1 [a]	165 ± 3 [a]	75 ± 6 [a]	90 ± 4
TL_flat	127 ± 1 [a]	135 ± 1 [a]	85 ± [a] 1	50 ± 1 [a]	FL_flat	105 ± 1 [a]	105 ± 1 [a]	46 ± 2 [a]	60 ± 2
TL_cylinder	134 ± 1 [a]	127 ± 3 [a]	78 ± 1 [a]	49 ± 2 [a]	FL_cylinder	154 ± 1	99 ± 1 [a]	95 ± 1 [a]	4 ± 1
TL_cone	159 ± 3	151 ± 1 [a]	92 ± 1 [a]	59 ± 1 [a]	FL_cone	156 ± 4	166 ± 3	129 ± 3 [a]	37 ± 3
TL_tulip	**166 ± 1**	**171 ± 1**	**142 ± 2**	**29 ± 1**	FL_tulip	147 ± 1	165 ± 4	134 ± 3 [a]	31 ± 3
TL_mushroom	**152 ± 1**	**156 ± 1**	**144 ± 4**	**12 ± 3**	FL_mushroom	149 ± 1	154 ± 1	132 ± 1 [a]	23 ± 1
TL_M. mouse	156 ± 1	152 ± 1	111 ± 4 [a]	41 ± 3 [a]	FL_M. mouse	149 ± 1	155 ± 4	127 ± 8 [a]	28 ± 6
TL_cubic	152 ± 1	168 ± 2	124 ± 1 [a]	44 ± 2 [a]	FL_cubic	145 ± 1	155 ± 1	107 ± 3 [a]	48 ± 2
TL_pyramid	156 ± 1	165 ± 2	56 ± 3 [a]	109 ± 3 [a]	**FL_pyramid**	**157 ± 1**	**157 ± 2**	**136 ± 2**	**20 ± 2**
TL_spiral	151 ± 1	160 ± 1	51 ± 3 [a]	110 ± 2 [a]	FL_spiral	154 ± 1	168 ± 2	105 ± 1 [a]	63 ± 1
TL_sphere	154 ± 1	159 ± 1	129 ± 1 [a]	30 ± 1	FL_sphere	155 ± 1	155 ± 2	107 ± 1 [a]	48 ± 1
TL_pine	108 ± 2 [a]	117 ± 1 [a]	78 ± 1 [a]	39 ± 1 [a]	FL_pine	128 ± 3 [a]	133 ± 1 [a]	120 ± 1 [a]	13 ± 1

[a] Wenzel regimen; θ_s = static CA; θ_A = advancing CA; θ_R = receding CA; θ_H = hysteresis CA, measured by the increment-decrement method.
Printing orientation: T = tilted, F = flat (horizontal)
Printing resolution: H, M, L = high, medium and low, respectively.

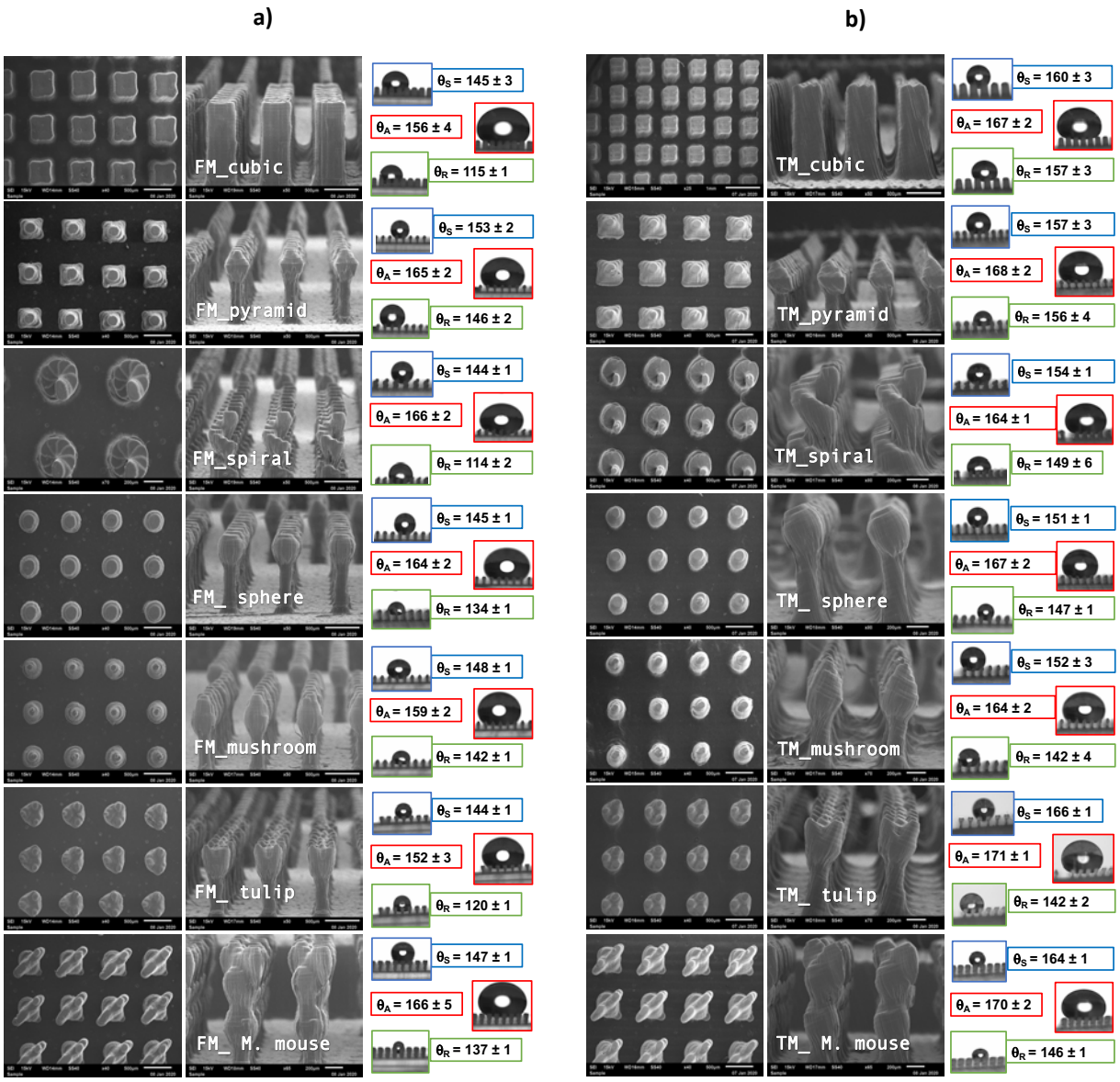

Fig. S2. Micrographs by SEM and their CAs values corresponding to silanized μ-PLS 3D printed at medium resolution: a) horizontal orientation, b) tilted orientation.

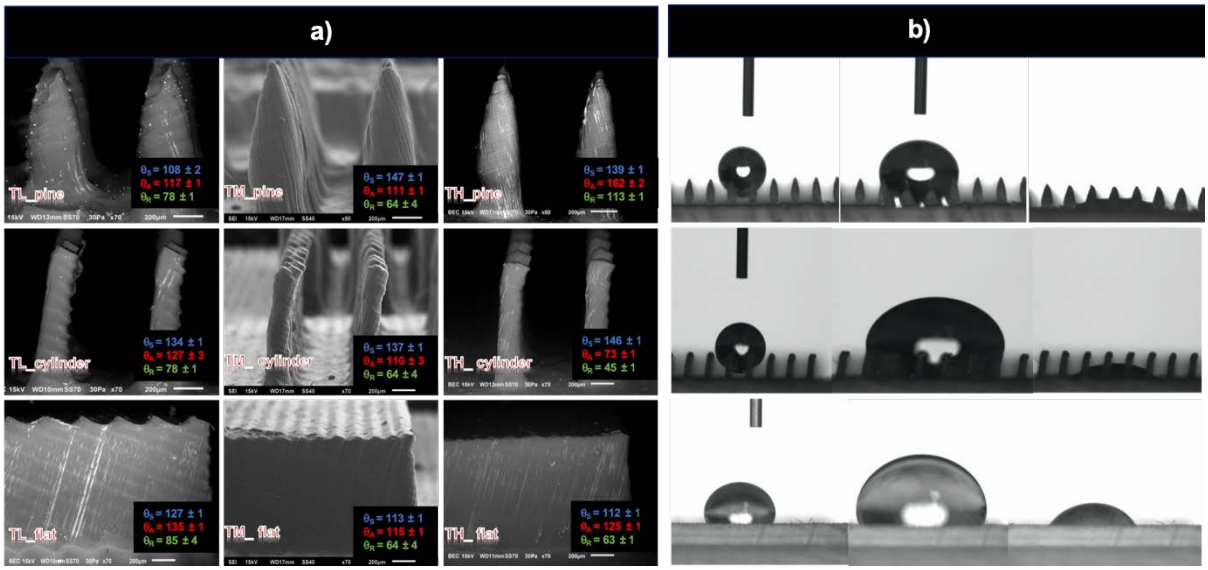

Fig. S3. a) Micrographs by SEM of silanized micro-PLS 3D-printed at tilted orientation and three printing resolutions (low, medium, and high), corresponding to geometrical shapes like a pine, cylindrical, and flat surfaces. **b)** Contact angle pictures corresponding to static, advancing, and receding contact angles. This behavior was observed regardless of the printing resolution.

Geometrical shapes with a sharp shape (pine) or with a cylindrical shape did not show a Cassie-Baxter regimen when the contact angles were measured. Nonetheless, they supported the droplet, which showed good sphericity to get a value of static CAs. When the size of the droplet was increased to measure the advancing CAs, it touched the base surface to reach the Wenzel regimen, as shown **in Fig. S1b**. Flat surfaces exhibited a Wenzel regimen regardless of the printing resolution.